



ELSEVIER

Available online at www.sciencedirect.com

SCIENCE @ DIRECT®

Journal of Magnetism and Magnetic Materials 301 (2006) 336–342

Journal of
magnetism
and
magnetic
materials

www.elsevier.com/locate/jmmm

Synthesis and characterisation of silica encapsulated cobalt nanoparticles and nanoparticle chains

A.S. Eggeman^{a,*}, A.K. Petford-Long^a, P.J. Dobson^b, J. Wiggins^b, T. Bromwich^a,
R. Dunin-Borkowski^c, T. Kasama^c

^a*Department of Materials Science, Oxford University, Parks Road, Oxford OX1 3PH, UK*

^b*Begbroke Science Park, Oxford University, OX5 1PF, UK*

^c*Department of Materials Science, Cambridge University, CB2 3QZ, UK*

Received 12 May 2005; received in revised form 24 June 2005

Available online 19 August 2005

Abstract

Nanoparticles of cobalt were produced by direct reduction in aqueous solution. These were subsequently coated in silica by a very slow hydrolysis reaction. Electrostatic and magnetic forces between the nanoparticles led to ordered structures forming, which were analysed by high resolution transmission electron microscopy. SQUID magnetometry showed that the nanoparticles were ferromagnetic with an additional magnetic signal from highly disordered surface states. Off-axis electron holography of the structures was undertaken and gives evidence for the mechanism by which the structures form.

© 2005 Elsevier B.V. All rights reserved.

Keywords: Nanoparticles; Core shell; SQUID magnetometry; Electron holography

1. Introduction

There has recently been a large amount of work investigating both synthesis and properties of magnetic nanoparticles. Interest in these materials comes from the diverse applications of magnetic

particles; these range from biomedical uses such as drug delivery [1] or magnetophoresis of specific biological entities [2] to recording media [3] to magnetic sealing systems [4].

Nanotechnology concerns itself with the ability to manipulate fully the properties of nanostructured materials, via their size, shape and composition [5–7], and also to develop reproducible, complex structures from simpler systems [8–10]. This can apply to magnetic nanoparticle systems, in which the nanoparticles often need to be incorporated

*Corresponding author. Tel.: +44 1865 273700;
fax: +44 1865 273789.

E-mail address: alexander.eggeman@materials.ox.ac.uk
(A.S. Eggeman).

into more complex structures to allow specific properties to be harnessed, or to adapt the particles for a specific application or environment.

Synthesis of metal nanoparticles has been achieved by a variety of different methods including colloid chemistry [11,12], cluster source deposition [13] and even mechanical milling [14]. One important factor in colloid chemistry routes is the role of the surfactant in controlling the size and monodispersity of the particles and in stabilising their surfaces to make particles with homogeneous surface chemistry; the surfactant can also allow further engineering of the particle surface [9]. One common technique is to use a surfactant that makes the particle surface vitreophilic [15]; a stabilising surface layer of an inert ceramic, such as silica or alumina, can then be grown. This can provide not only a barrier to environmental corrosion [16], but can also create a barrier against particle agglomeration [17].

The size of a magnetic nanoparticle is very important in determining its magnetic properties. Magnetic domains have a finite size, and there is thus a critical nanoparticle diameter (d_c) below which only a single stable domain can be supported. This is given by [18]

$$d_c \approx 18 \frac{(AK_u)^{1/2}}{\mu_0 M_s^2},$$

where A is the exchange stiffness constant, K_u is the magnetocrystalline anisotropy constant, μ_0 is the permeability of free space and M_s is the saturation magnetisation. Nanoparticles with a diameter below d_c can reverse their magnetisation only by magnetic moment rotation and so are magnetically harder than particles with a diameter above d_c . Additionally there is a particle size at which the stabilising magnetic energy of the particle is equal to the thermal energy of the environment. Below this size the magnetisation of the particle can be reversed by thermal energy and so the particles show no net magnetisation. This is defined by [18]

$$K_u V = 25k_B T,$$

where V is the particle volume, k_B is Boltzmann's constant and T is temperature. Cobalt is of particular interest because in the hexagonal form

it has a large anisotropy constant. This means that a range of cobalt nanoparticle sizes can be investigated before stable magnetic domains can form and the particles exhibit bulk magnetic properties. For example, the single domain limit for cobalt has been calculated as 70 nm [19], whereas the superparamagnetic limit for hcp cobalt is approximately 2 nm. In this paper we report the formation of magnetic nanostructures based on cobalt nanoparticles with a silica coating.

2. Experimental

The cobalt particles were produced using a direct reduction. Sodium borohydride was dissolved in 100 mL of de-aerated, de-ionized water to produce a 0.01 M solution; to this was added a varying amount of citric acid; creating a solution of between 0.1 and 0.25 mM concentration. To this 100 μ L of 0.4 M $\text{CoCl}_2(\text{aq})$ was added under ultrasonication to allow rapid mixing. The solution rapidly changed from pale pink to pale grey as the cobalt nanoparticles were formed. After a few seconds 30 mL of the nanoparticle solution was withdrawn and added to a 200 mL de-aerated ethanolic solution containing 5 μ L of 3-aminopropyltriethoxysilane (APS) and 15 μ L of tetraethylorthosilicate (TEOS) for silica deposition overnight [20].

Size and morphological characterisation was undertaken on a JEOL 4000EX set up for dedicated HREM, this operates at 400 KV. Magnetic measurements were taken on an MPMS superconducting quantum interference device (SQUID). Off-axis electron holography was performed in a Philips CM300ST field emission gun TEM equipped with a "Lorentz" lens and a GatanTM image filter (GIF). This operates at 300 KV and the operation is described in more detail later.

3. Results and discussion

The simple process of synthesising nanoparticles and then coating them discretely with silica proved to be an oversimplification. The first samples made

by this procedure consisted of agglomerated nanoparticles with a coating of silica of approximately 50 nm in thickness, a typical example of which is shown in the transmission electron microscope (TEM) image seen in Fig. 1a. The size distribution of these particles was quite wide, suggesting that the nucleation and growth of the particles could be controlled to a greater extent. This was done by altering the concentration of surfactant, to control the growth of the particles or by altering the reducing conditions of the reaction to create a more controlled particle-nucleation.

Figs. 1b and c show the effect of reducing the surfactant concentration (from 0.25 to 0.1 mM) (b); and increasing the concentration of reducing agent (from 0.1 to 0.5 M) (c) in the reaction mixture. The change in size and monodispersity of the nanoparticles has led to a change in the way that they cluster and combine, with them now forming chain structures encapsulated in 15–20 nm of silica. All of the particles imaged in the TEM seemed to be incorporated within these chain structures, there may have been a small number of “free” nanoparticles but there is no TEM evidence of these.

From the electron micrographs, particle analysis of the two chain samples was possible. In Fig. 1b, the mean nanoparticle diameter is 27.4 nm with a standard deviation (σ) of 8.3 nm, in Fig. 1c the nanoparticles produced at a higher borohydride concentration have a mean diameter of 22.0 nm with $\sigma = 8.0$ nm. This, however, is not the entire situation, as the morphology of the chains is quite

well defined. In all of the chains imaged in the TEM, at least one end of the chain is bounded by a much larger nanoparticle, with these removed the remaining nanoparticles comprising the chain length are much more monodisperse. In the low borohydride sample (Fig. 1b) the average chain particle diameter is 25.0 nm with $\sigma = 4.0$ nm and the higher borohydride sample the mean chain particle diameter is 19.7 nm with $\sigma = 2.3$ nm. In both cases, samples of over 200 particles were used.

It seems that the decrease in surfactant concentration has allowed the particles to continue growing for a longer time before the particle surface becomes stabilised against further growth. The increased reducing agent concentration seems to have resulted in a faster nucleation rate, with less subsequent particle growth, leading to a higher monodispersity of the particles.

The electron diffraction pattern of the samples, shown in inset in Fig. 1c, suggests that the cobalt produced takes the fcc structure. The first strong ring corresponds to a $\{111\}$ reflection with diffuse and weak rings corresponding to $\{200\}$ and $\{202\}$. The rings are more diffuse than would be expected for 20 nm particles, which can be explained if the particles are composed of highly disordered crystallites rather than being single crystal; indeed, other material produced by this method was described as amorphous [20] because of the lack of strong diffraction.

SQUID magnetometry was used to analyse the temperature response of the magnetic properties of

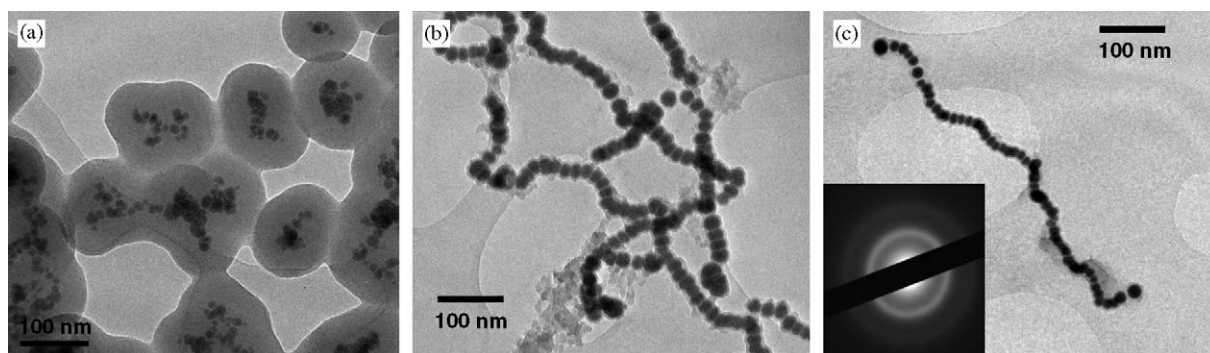


Fig. 1. Electron micrographs of (a) encapsulated nanoparticle clusters; (b) and (c) encapsulated nanoparticle chains.

the chains of nanoparticles. Field cooled (FC) and zero-field cooled (ZFC) measurements were taken of the higher borohydride sample shown in Fig. 1c to investigate the temperature-dependent transition in the magnetic properties. Hysteresis loops were also recorded at 20 K and at room temperature.

The FC and ZFC data, shown in Fig. 2a, are almost identical, which suggests that the particles are in fact ferromagnetic. Fig. 3 shows the data in the region of the curve between 75 and 300 K, plotted as $M(T)/M(0)$ against T/T_c with an extrapolated value of $M(0) = 1.89 \times 10^{-4}$ emu and $T_c = 1000$ K. The lower value of T_c is not unreasonable given the particle size and the degree of disorder [21,22]. The curve closely follows the

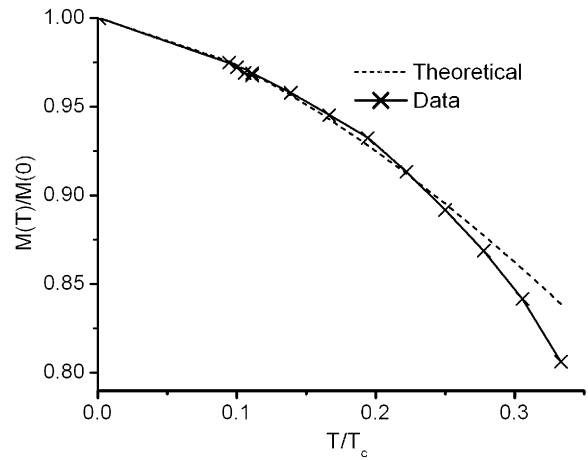


Fig. 3. Magnetisation as a function of temperature.

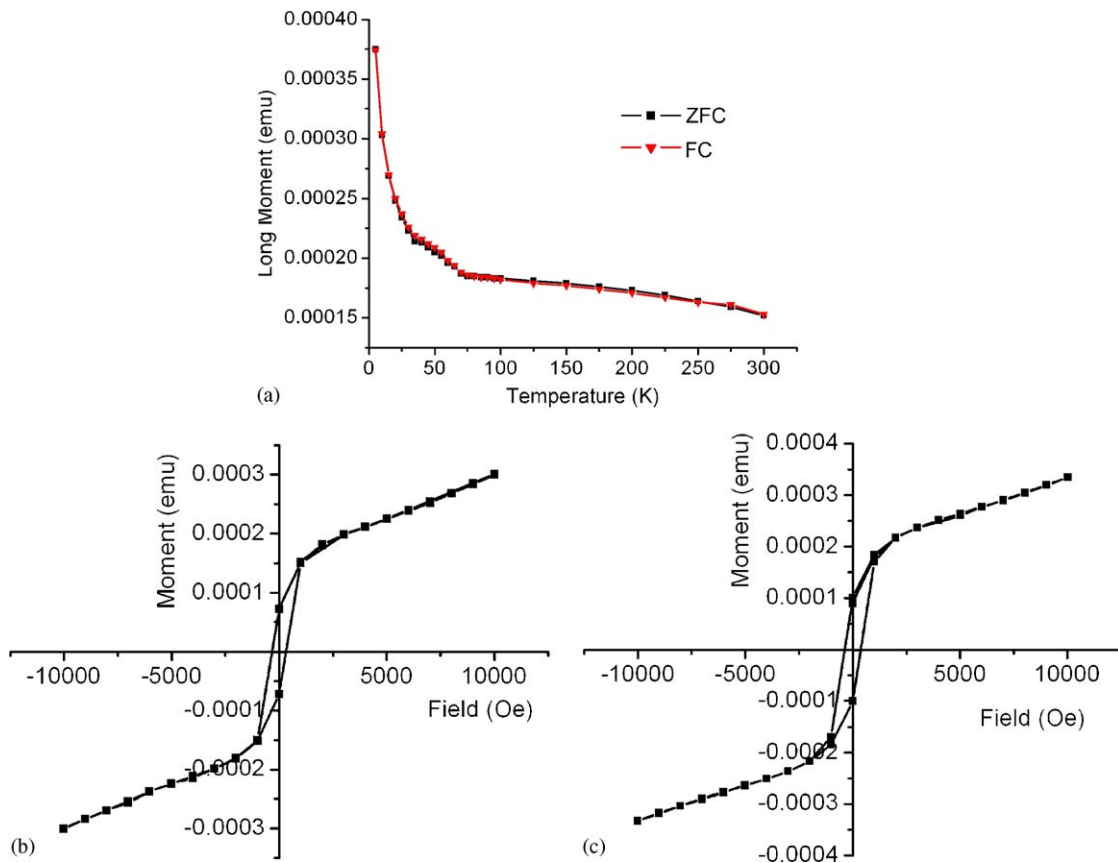


Fig. 2. SQUID magnetometry data. (a) FC–ZFC curves; (b) and (c) hysteresis curves at 300 K and 20 K, respectively.

$T^{3/2}$ decay behaviour predicted for a ferromagnet at low temperatures by the classical molecular field theory. At higher temperatures the recorded data tend more towards the T^2 decay as predicted also by this theory [18].

With this ferromagnetic signal removed from the curve there remains a component that rapidly decays from 5 to 35 K; this component is identified by Δ in Fig. 4.

There are two possible explanations for this; firstly the smaller particles could be superparamagnetic, and the curve shape is caused by thermally assisted moment rotation. The other possibility is that the additional magnetic component is caused by surface states with a disordered spin structure, whose magnetisation decreases much more rapidly with temperature than “bulk-like” states [23,22]. The electron diffraction pattern in Fig. 1c suggests that the particles are highly disordered, this means that there is likely to be significant amounts of material exhibiting these spin structures; additionally the absence of decreased magnetisation in the low temperature region of the ZFC curve suggests that the particles are not superparamagnetic and that the disordered material is responsible.

The remaining region of the curve (between 35 and 70 K) is harder to explain. It is possibly caused by the presence of a small number of particles not associated with a chain. The feature can be fitted

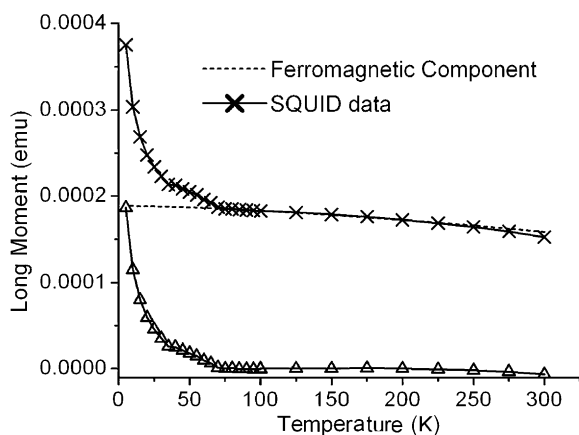


Fig. 4. Separation of the SQUID data into ferromagnetic and additional components.

to a similar curve to that shown in Fig. 3, with a lower T_c ; the small size of the nanoparticles and their disordered structure could allow this to be the case. Such particles were not observed by TEM but the sampled volume in the SQUID is much larger than that seen in TEM.

The two hysteresis loops in Fig. 2b and c confirm that the overall magnetic signal is ferromagnetic as there is little change between the low temperature and room temperature curves. Additionally they show that there is no cobalt oxide present. Cobalt oxide is an antiferromagnet and its presence would offset the hysteresis loops, which has not been seen for any of the samples. The corrosion resistance of the silica coating is such that the samples produced show little or no degradation after several months of storage.

Further magnetic analysis was performed in a TEM using off-axis electron holography. This involves creating an interference pattern in a TEM between two parts of a split electron beam. One passes through the sample and the other passes through empty space. A phase shift is introduced by the in-plane component of the magnetic induction and by the electrostatic potential of the sample. The two beam components are then re-converged by the introduction of a wire carrying a positive bias; this acts as an electron bi-prism allowing the formation of an electron hologram [24,25]. The common means of expressing the phase change data obtained from the electron hologram is as a colour map where different colours are assigned to different magnetic induction directions; additionally lines of constant phase change can be calculated. The hologram shown in Fig. 5 has the phase contours added.

Analysis of this image supports the conclusions drawn from the SQUID data. As can be seen, there are significantly larger particles at the end of the chains, as is observed in all of the chains imaged. The larger particles have a complex internal magnetic structure, and contain either a magnetic vortex [24] or multiple domains. By contrast, the particles in the rest of the chain show a much simpler structure. They have a uniform internal magnetisation, suggesting that they are single domain and are aligning fully along the

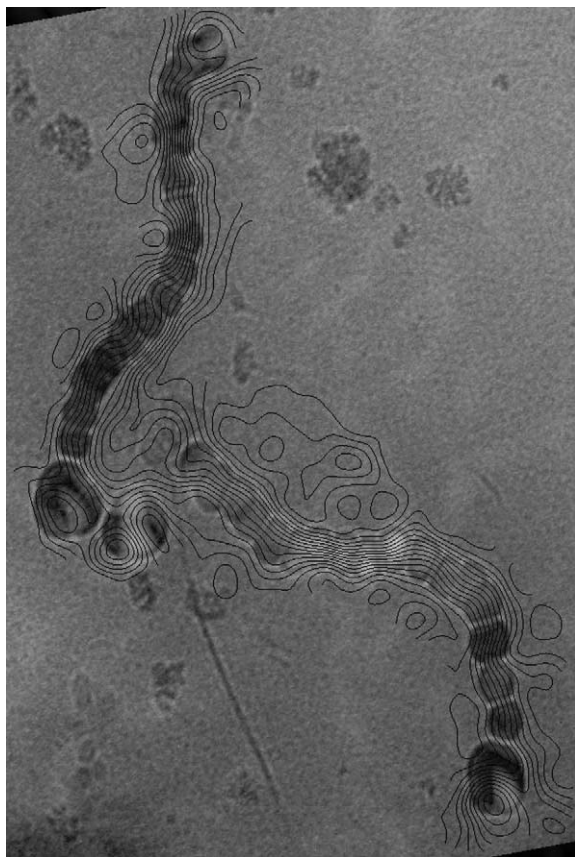


Fig. 5. Electron hologram of nanoparticle chains.

magnetic field of the end particles and the rest of the chain.

4. Conclusions

The evidence gathered thus far has led to the working hypothesis about how the chain structures form. The TEM images show quite clearly that the spatial distribution of the two particle sizes in the chains is quite regular; the larger particles lie at the ends of the chains with the smaller particles constituting the majority of the chain.

In the reaction vessel there will be a dilute sol of these particles, and it is thus feasible that a smaller particle will be attracted to close proximity with a

large particle as a result of its higher magnetic moment. The magnetic dipoles of the two particles will align, and the two particles will be attracted together. With these two particles now arranged together there would be an increased dipole because of the increased volume of material, thus attracting other particles. Given their higher population, these would most likely be the smaller particles. The new particle would more likely be attracted to the end of the chain of small particles rather than to the larger nucleus particle because the smaller particles are single domain and so exhibit higher stray field than the larger particles, which tend to form flux closure structures. In this way we see a stepwise growth of the chain. The growth of the silica is slow because the hydrolysis rate of TEOS due to water is low, which means that the encapsulation and stabilisation of the chains by silica will only occur long after the chain growth has stopped.

This method adequately explains the HREM and SQUID data and is supported by the electron holography data.

Acknowledgements

The authors would like to thank Dr Andrew Boothroyd and Dr Dharmalingam Prabhakaran of the Clarendon Laboratory, Oxford, for their assistance with the SQUID magnetometry.

References

- [1] Q.A. Panckhurst, J. Connolly, S.K. Jones, J. Dobson, *J. Phys. D* 36 (2003) R167.
- [2] P. Tartaj, M. del Puerto Morales, S. Veintemillas-Verdaguer, T. Gonzalez-Carreño, C.J. Serna, *J. Phys. D* 36 (2003) R182.
- [3] S. Sun, C.B. Murray, D. Weller, L. Folks, A. Moser, *Science* 287 (2000) 1989.
- [4] K. Raj, R. Moskowitz, *J. Magn. Magn. Mater.* 85 (1990) 233.
- [5] E. Matijević, *J. Appl. Chem.* 64 (1992) 1703.
- [6] E. Matijević, *Langmuir* 10 (1994) 8.
- [7] M.P. Pileni, C. Petit, *J. Magn. Magn. Mater.* 166 (1997) 82.
- [8] P. Mulvaney, L.M. Liz-Marzan, M. Giersig, T. Ung, *J. Mater. Chem.* 10 (2000) 1259.
- [9] F. Caruso, *Adv. Mater.* 13 (2001) 11.

- [10] M. Paulose, C.A. Grimes, O.K. Varghese, E.C. Dickey, *Appl. Phys. Lett.* 81 (2002) 153.
- [11] E. Matijevic, D.V. Goia, *New J. Chem.* 22 (1998) 1203.
- [12] T. Hyeon, *Chem. Commun.* (2003) 927.
- [13] D.L. Peng, H. Yamada, T. Hihari, T. Uchida, K. Sumiyama, *Appl. Phys. Lett.* 85 (2004) 2935.
- [14] E. Bonetti, L. Del Bianco, S. Signoretti, P. Tiberto, *J. Appl. Phys.* 89 (2001) 1806.
- [15] T. Jesionowski, *Colloids Surf. A: Physicochem. Eng. Aspects* 222 (2003) 87.
- [16] R.H.M. Godoi, M. Jafellicci, *J. Magn. Magn. Mater.* 226 (2001) 1918.
- [17] J. Wagner, T. Autenrieth, R. Hempelmann, *J. Magn. Magn. Mater.* 252 (2002) 4.
- [18] R.C. O'Handley, *Modern Magnetic Materials: Principles and Applications*, Wiley Inter-Science, New York, 2000.
- [19] R.D. Rieke, D.L. Leslie-Pelecky, *Chem. Mater.* 8 (1996) 1770.
- [20] Y. Kobayashi, M. Horie, M. Konno, B. Rodriguez-Gonzalez, L.M. Liz-Marzan, *J. Phys. Chem. B* 107 (2003) 7420.
- [21] R.I. Khaibullin, et al., *J. Phys.: Condens. Matter* 16 (2004) L443.
- [22] X. Battle, A. Labarta, *J. Phys. D* 35 (2002) R15.
- [23] H. Kachkachi, M. Nogues, E. Tronc, D.A. Garanin, *J. Magn. Magn. Mater.* 221 (2000) 158.
- [24] M. Hytch, et al., *Phys. Rev. Lett.* 91 (2003) 257207.
- [25] R.E. Dunin-Borkowski, et al., *Science* 282 (1998) 1868.